Journal of Power Sources 268 (2014) 240–245

Contents lists available at ScienceDirect

Journal of Power Sources

journal homepage: www.elsevier.com/locate/jpowsour

Corrosion behavior of TiN, TiAlN, TiAlSiN-coated 316L stainless steel in simulated proton exchange membrane fuel cell environment

Nguyen Dang Nam [a, *], Mahesh Vaka [b], Nguyen Tran Hung [c]

[a] Petroleum Department, Petrovietnam University, Ba Ria City, Ba Ria – Vung Tau Province 74000, Viet Nam
[b] School of Life and Environmental Sciences, Deakin University, Victoria 3220, Australia
[c] Institute of Chemistry & Materials Science, 17 Hoang Sam, Ha Noi 10000, Viet Nam

HIGHLIGHTS

- Multicomponent TiAlSiN hard coating is deposited on 316L SS as bipolar plates for PEMFC.
- Electrochemical results indicate that the TiAlSiN coating has excellent corrosion resistance in PEMFC's environment.
- The TiAlSiN coating satisfies the quality requirement for BPs (<0.01 Ω cm^2).
- The TiAlSiN coating should be more conducting in cathode side of a PEMFC.

ARTICLE INFO

Article history:
Received 30 April 2014
Received in revised form
28 May 2014
Accepted 29 May 2014
Available online 7 June 2014

Keywords:
PEMFC
Bipolar plate
Multicomponent
Hard coating
Corrosion resistance

ABSTRACT

To gain high hardness, good thermal stability and corrosion resistance, multicomponent TiAlSiN coating has been developed using different deposition methods. In this study, the influence of Al and Si on the electrochemical properties of TiN-coated 316L stainless steel as bipolar plate (BP) materials has been investigated in simulated proton exchange membrane fuel cell environment. The deposited TiN, TiAlN and TiAlSiN possess high hardness of 23.9, 31.7, 35.0 GPa, respectively. The coating performance of the TiN coating is enhanced by Al and Si addition due to lower corrosion current density and higher $R_{coating}$ and R_{ct} values. This result could be attributed to the formation of crystalline-refined TiN(200), which improves the surface roughness, surface resistance, corrosion performance, and decreased passive current density.

1. Introduction

Polymer electrolyte membrane fuel cells (PEMFCs) can be used as a major clean power source in the near future due to their high power density at relatively low operating temperatures (<100 °C) [1,2]. Moreover, the acceptable cost of PEMFCs is a significant issue in their commercial applications. Among the PEMFC components, the bipolar plates maintain a pretty large proportion of the volume, total weight and cost [3]. Therefore, by investigating highly conducting BP materials both weight and volume reductions will impact directly on improving the power density and reducing the cost of PEMFCs. Hermann et al. have suggested the criteria and properties for BPs: electrical conductivity – plate resistance <0.01 Ω cm^2, high thermal conductivity, hydrogen/gas permeability $<10^{-4}$ cm^3 s^{-1} cm^{-2}, corrosion resistance – corrosion rate <0.016 mA cm^{-2}, compressive strength >0.15 MPa and density <5 mg cm^{-3} [4].

The materials majorly used for BPs to-date consist of non-metals (graphite and electrographite), metals (uncoated and coated) and composites (carbon-composite and metal-composite). Graphite and its composites have been used as BPs with a high chemical stability and low surface contact resistance. But, they have high gas permeability, relatively high cost, brittleness and low power density which are the main limitations to its more widespread use [5]. Metallic materials such as stainless steels [6–9], titanium [6,10] and nickel [11,12] have been chosen as BP material candidates due to a set of properties for the design and elaboration of compact, light and cheap bipolar plates. However, corrosion damage is still seen due to the acidic media (pH 3–4) and temperature conditions (around 80 °C). It is also involved in MEA pollution by metal cations

* Corresponding author. Tel.: +84 643 738 879; fax: +84 643 733 579.
E-mail addresses: namnd@pvu.edu.vn, ndnam12a18@yahoo.com (N.D. Nam).

http://dx.doi.org/10.1016/j.jpowsour.2014.05.144
0378-7753/

dissolution during corrosion processes. Among the metallic candidates chosen for BP materials, stainless steels have been tremendously used as common material because of their relatively high chemical stability, high strength, low corrosion rate and low gas permeability [13]. However, one of the main concerns of stainless steel is the contact resistance of the surface film as a result of power loss [6,14]. The properties of stainless steel suitable for BPs in PEMFCs have been improved by surface modification. To improve stainless steel's interfacial contact resistance values, various coatings were applied using titanium nitride [15–19], chromium nitride [12,20–23], chromium and titanium nitride multi coating [24–28], and conducting polymer [29–33].

On account of its good corrosion resistance for PEMFC application, mechanical properties and contact resistance, TiN is a promising candidate as coating material [24–28]. TiN hard coatings obtained by magnetron sputtering physical vapor deposition (PVD) method have been used for increasing the corrosion resistance of the substrate. Nevertheless, the substrate can be exposed to aggressive environments due to the presence of pores and pinholes on the surface of the TiN coating, which reduces its protective ability. Recently, multicomponent TiAlSiN hard coating provides the benefit of individual components leading to a further improvement of TiN and TiAlN coating properties [34–37]. Multicomponent TiAlSiN coating has a small amount of Si consisting of single B1 cubic phase and grain refinement. In addition, the pores and pinholes could be removed due to the formation of nanocrystalline TiAlN and amorphous silicon nitride. Furthermore, good thermal stability, hardness and oxidation resistance was significantly improved due to the Si-rich oxides acted as a diffusion barrier for further oxidation [38,39]. In this study, therefore, the work focused on evaluating the electrochemical behavior of TiN, TiAlN and TiAlSiN coatings prepared by cathodic arc plasma system as a function of Al and Si addition. The corrosion resistance of these coatings was investigated in a simulated cathode environment of PEMFC in order to improve the protective ability and obtain basic information for the development of TiAlSiN coatings as BP material candidates.

2. Experimental

2.1. Preparation of materials

A type 316L (a diameter of 20 mm and a thickness of 3 mm) stainless steel substrate was used for the coating to be deposited. The stainless steel compositions were checked by Optical Emission Spectroscopy and results obtained are as follows: 0.02% C, 0.76% Si, 1.66% Mn, 17.16% Cr, 2.2% Mo, 10.81% Ni, 0.41% P, 0.025% S, 0.085% N. TiN, TiAlN and TiAlSiN coatings were deposited on 316L SS substrates using the cathodic arc plasma system. Typically, TiN, TiAlN and TiAlSiN coatings were deposited under nitrogen reactive gas, base and working pressures of 1.3×10^{-4} and 4 Pa, respectively. High purity Ti (99.9%), Al (99.8%), AlSi (88% Al and 12% Si) were used as cathode targets. A bias voltage of −150 V was used as substrate bias voltage at 300 °C of substrate temperature. 55 A for Ti, 45 A for Al and AlSi were used as the target currents. 4.55 rpm and 280 mm were used as rotational velocity of substrate and cathode and substrate distance. An approximately 1.5 μm-thick TiN, TiAlN, and TiAlSiN was deposited on the 316L SS substrate.

The coating thicknesses and compositions were confirmed using SEM/EDS Supra 55 VP and electron probe micro-analyzer (AFM) using Bruker Multimode 8. The crystal structure of the as-received specimens was examined by X-ray diffraction (XRD) using CuKα radiation. XRD data was measured by Model D/MAX-RC equipment. The scan range of the 2 theta was from 30° to 90°. In addition, the surface resistance was also measured using a four-point probe method using CM21205 (Chang Min Co., Ltd) before and after potentiostatic tests. In order to get the average value, at least three times for each specimen were measured. Hardness of the coating were obtained using XP-MTS nano-indentation with a Berkovich indenter, under load–unloading condition, and measured as a function of indenter displacement using continuous stiffness measurement method. To avoid the influence of substrate on the measured hardness, the maximum penetration depth was controlled at 250 nm.

2.2. Electrochemical tests

All experiments were performed at 70 °C in a 1 M H_2SO_4 + 2 ppm F^- with pressurized air purging at a flow rate of 1.0 dm^3 min^{-1}. The exposed coating area was 1 × 1 cm^2. The electrochemical polarization tests were performed using a VSP system (BioLogic Scientific Instruments). Saturated calomel and pure graphite were used for the reference and counter electrodes, respectively. Prior to the potentiodynamic polarization test, the samples were kept in the solution for 3 h to establish the open-circuit potential. The potential of the electrodes was swept from an initial potential of −250 mV vs. corrosion potential (E_{corr}) to a final potential of 1000 mV_{SCE} at a rate 0.166 mV s^{-1}. Electrochemical

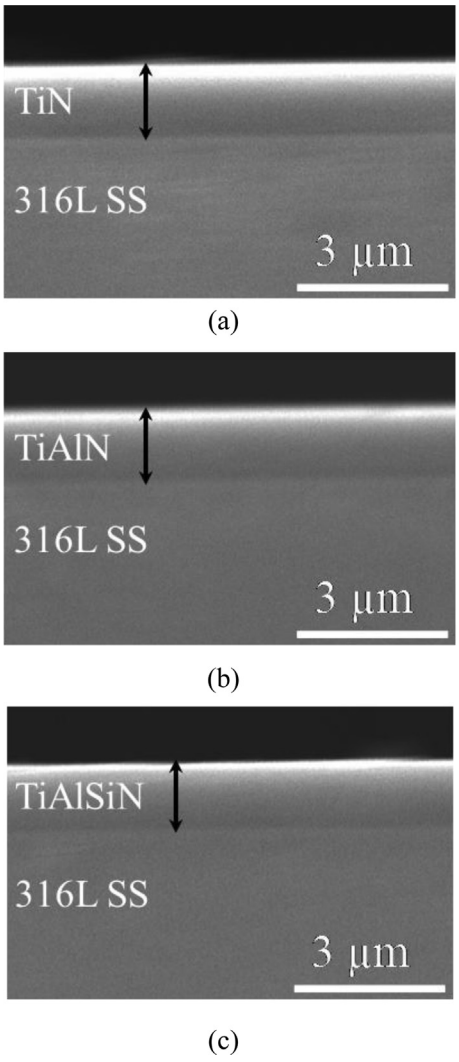

Fig. 1. Cross section of (a) TiN, (b) TiAlN and (c) TiAlSiN coatings.

Table 1
Chemical composition (at.%) of coatings.

Specimen	Ti	Al	Si	N
TiN	50.31	–	–	49.69
TiAlN	26.90	25.89	–	47.21
TiAlSiN	25.17	19.01	2.81	53.01

impedance spectroscopy (EIS) tests were conducted using a VPS system with a commercial software program for the AC measurements. A peak to peak amplitude of the sinusoidal perturbation signals of 10 mV was used. The frequency ranged from 100 kHz to 10 mHz. The model VSP system of BioLogic scientific instruments was also used to apply +600 mV_{SCE} to simulate the cathodic environment of a PEMFC.

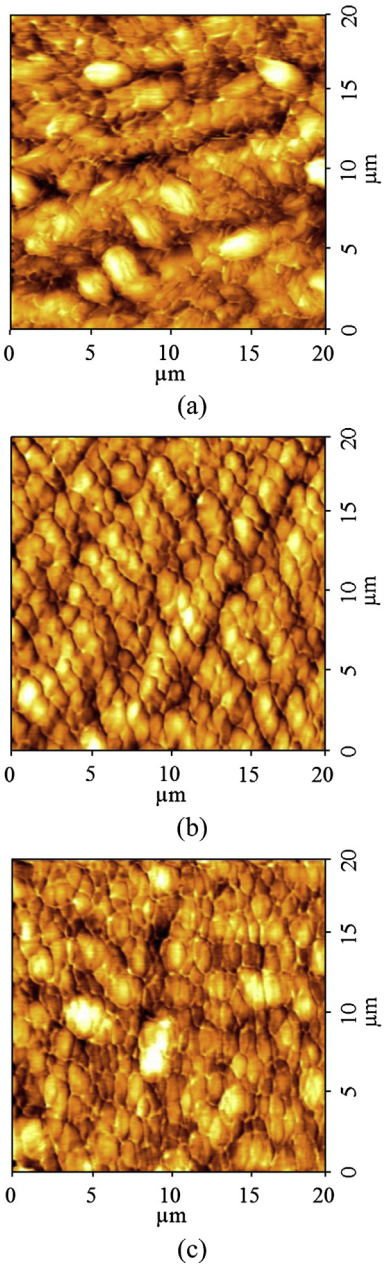

Fig. 2. AFM images showing the uniformity of (a) TiN (9.15), (b) TiAlN (5.67) and (c) TiAlSiN coatings (4.5 μm).

3. Results and discussion

3.1. Structure and composition

Fig. 1 shows the cross section images of the TiN, TiAlN and TiAlSiN-coated 316L SS. It indicates that all coating thicknesses were approximate 1.5 μm and also compared with Alpha-Step method. In addition, the chemical compositions of the deposited TiN, TiAlN and TiAlSiN coating are presented in Table 1. The nitrogen content of all the deposited coatings was 47.21 at.% – 53.01 at.%. The TiAlSiN quaternary alloy coating Ti/(Ti + Al + Si) ratios being 0.53 were deposited to obtain optimal mechanical properties [40–43]. Fig. 2 shows the coating surface roughness of the as-deposited specimens. Coating roughness (R_{rms}) values of 9.2, 5.7 and 4.5 nm were determined for TiN, TiAlN and TiAlSiN by AFM, respectively. This indicates that the difference in surface roughness was small and the coating surface roughness of the TiN films decreased with the Al and Si incorporation. The nanocomposite microstructure could be demonstrated by the formation of a face-centered cubic (Ti,Al)N phase, obtained by

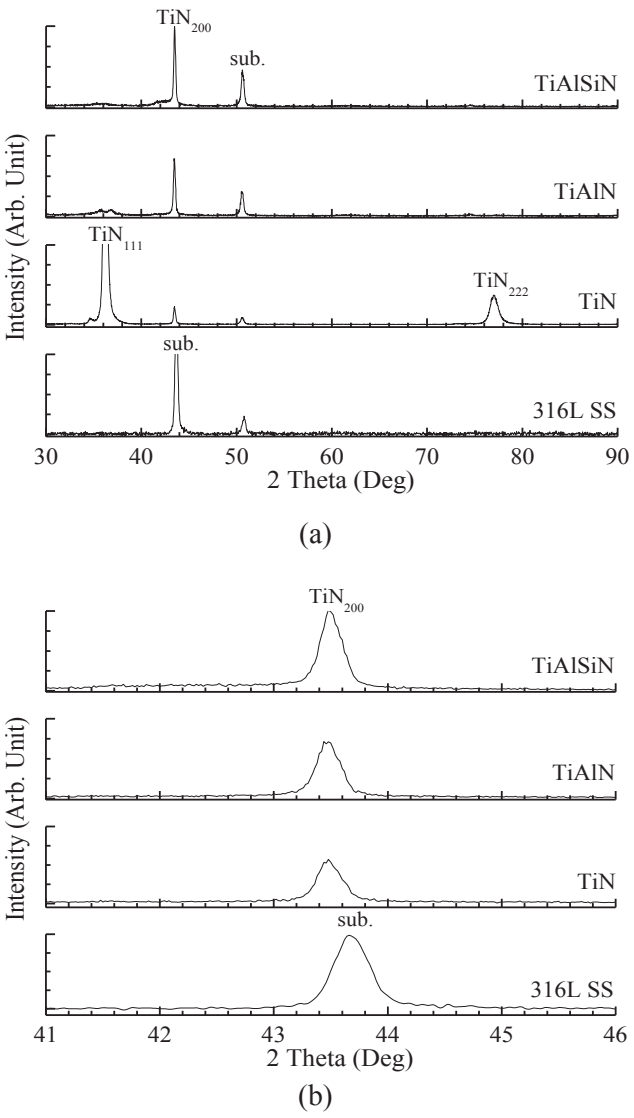

Fig. 3. XRD patterns of the TiN, TiAlN and TiAlSiN coatings: (a) full scan and (b) TiN(200) narrow scan.

substitution of Al in the cubic titanium nitride phase, and an amorphous matrix at the column boundary regions mainly composed of Si and N [40,44,45]. Therefore, a smoother surface is observed.

Fig. 3 shows the XRD patterns of 316L SS, TiN, TiAlN and TiAlSiN coatings, respectively. The TiN film showed multiple orientations of (111), (200) and (222) crystal planes appeared and the strongest orientation was TiN(111) plane. As Al and Si were incorporated into TiN film, a strong preferred orientation of the (200) crystal plane was obtained and highest (200) peak was observed in the TiAlSiN coating. That means that TiAlSiN coating has a preferred (200) orientation as compared to TiN and TiAlN coatings. Thus, Containing Si into the coatings facilitated (200) growth orientation. It could be related to the diminution of the grain size and/or the residual stress induced in the crystal lattice [46]. This result corresponds to the results of AFM and indicates that more high-quality TiN films may be deposited using Al and Si incorporation. In addition, the hard coating layer formed on the stainless steel surface increased the hardness. In particular, TiAlSiN film showed considerable enhanced hardness which can be attributed to the crystal size refinement due to the incorporation of Si in accordance with the Hall–Petch relationship [47,48]. Even though the incorporation of Al was also expected to increase the hardness on the basis of the Hall–Petch effect, the result of TiAlN film was slightly lower than that of TiN film presumably due to the localized formation of soft wurtzeit-like hexagonal AlN structures. The nanocomposite microstructure could be formed at the column boundary regions mainly composed of Si and N and decrease the mobility of dislocations. Furthermore, Carvalho et al. [34], Zhang and Ali [35], Rafaja et al. [36], Holubar et al. [37] also reported that the multicomponent TiAlSiN hard coating exhibited nanostructured composite microstructures including solid-solution (Ti, Al, Si)N crystallites and amorphous Si_3N_4. The Si addition resulted in the grain refinement of (Ti, Al, Si)N crystallites and its uniform distribution with percolation phenomenon of amorphous silicon nitride. Thus, an increase in coating hardness has been obtained (see Fig. 4).

Fig. 5 shows the surface resistance of the TiN, TiAlN and TiAlSiN coatings. There was a transition from a higher surface resistance to a lower value after the application of potential, which indicates an improved electric conductivity at +600 mV_{SCE} application. The TiN, TiAlN and TiAlSiN coatings clearly showed good electrical conductivity for cathode BP application. All the coatings demonstrated low electrical resistance and satisfied the quality requirement for BPs (<0.01 Ω cm^2 [4]).

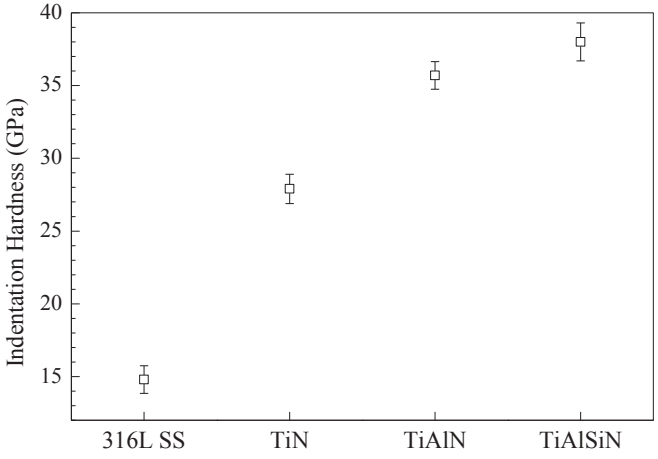

Fig. 4. Coating hardness of the deposited TiN, TiAlN and TiAlSiN coatings.

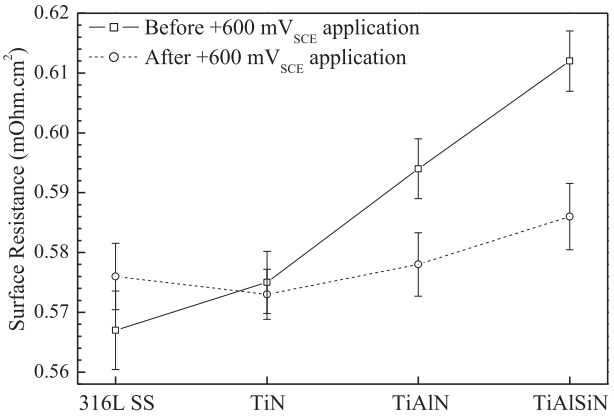

Fig. 5. Surface resistance of the coatings before and after +600 mV_{SCE} application.

3.2. Corrosion resistance

Fig. 6(a) shows the potentiodynamic polarization curves of uncoated and TiN, TiAlN and TiAlSiN-coated 316L stainless steel specimens. The multicomponent hard coatings increased the corrosion resistance with low corrosion current densities ranging from 0.5 to 1.8 μA cm^{-2}. The current densities were lower than that

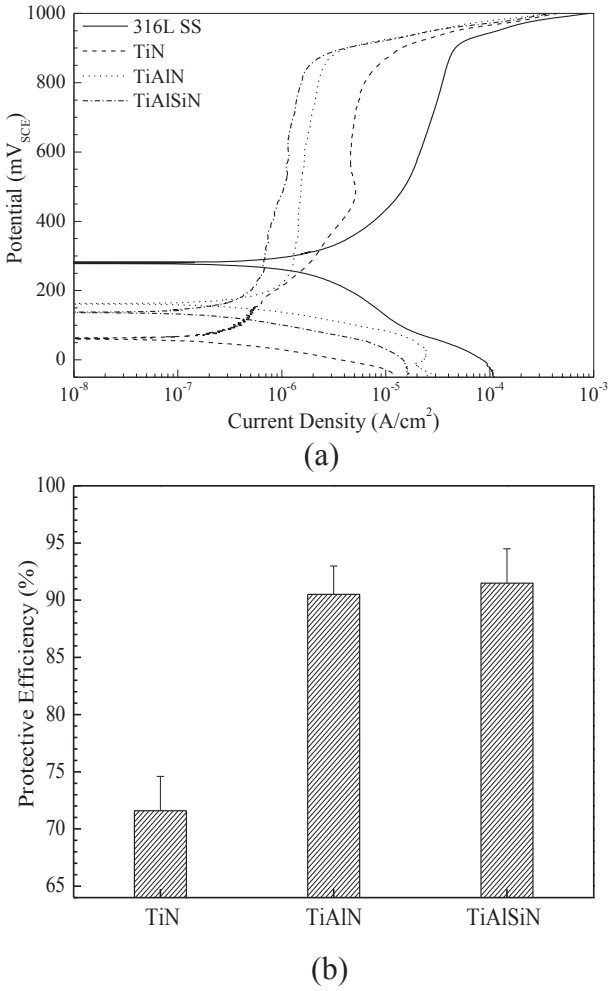

Fig. 6. (a) Polarization curves of TiN, TiAlN and TiAlSiN-coated 316L stainless steel and (b) comparison of protective efficiency of the coatings.

Table 2
Corrosion properties obtained from the polarization curves.

Specimen	E_{corr} (mV_{SCE})	i_{corr} ($\mu A\ cm^{-2}$)	β_a ($mV\ decade^{-1}$)	β_c ($mV\ decade^{-1}$)
316L SS	278	6.3	190	177
TiN	63	1.8	170	49
TiAlN	164	0.7	154	87
TiAlSiN	140	0.5	141	76

of the substrate, where a passivation region had formed. There was no pitting observed up to 1000 mV_{SCE}. The rapid increase in current density at approximately +900 mV_{SCE} was attributed to the anodic current density associated with oxygen evolution due to water dissociation [20,33]. However, all the multicomponent hard coating specimens and 316L SS had a passivation range for a cathodic working potential of +600 mV_{SCE} at a very low current density. Table 2 shows the corrosion properties of the 316L SS substrate and multicomponent hard coatings as a function of the Al and Si addition obtained from the polarization test. The protective efficiency (P_i) of the coatings was determined using the following equation [49]:

$$P_i = 100 \times \left(1 - \frac{i_{corr}}{i^o_{corr}}\right) \quad (1)$$

where i_{corr} and i^o_{corr} are the corrosion current densities in the presence and absence of a coating, respectively. The electrochemical characteristics of the multicomponent hard coatings showed better coating performance with a lower passive current density in comparison with 316L SS substrate. Fig. 6(b) shows that the protective efficiency of the coatings was quite high and increased when Al and Si added to TiN film, with the highest protective efficiency of 95% being achieved in case of multicomponent hard TiAlSiN coating.

Under real PEMFC working conditions, the cathode works at a potential of approximately +600 mV_{SCE}. Therefore, the corrosion behavior of metallic bipolar plates under real PEMFC conditions was examined by carrying out the potentiostatic tests at +600 mV_{SCE} purged with O_2. Fig. 7 shows the potentiostatic measurements at +600 mV_{SCE} in 1 M H_2SO_4 + 2 ppm F^- (70 °C) purged with air. After the specimen reached a stable OCP, a potential was applied and the current density was recorded for 168 h. The current densities of the multicomponent hard coating specimens remained at a very small values compared with the substrate. This suggests that the coatings protected the 316L SS from pitting

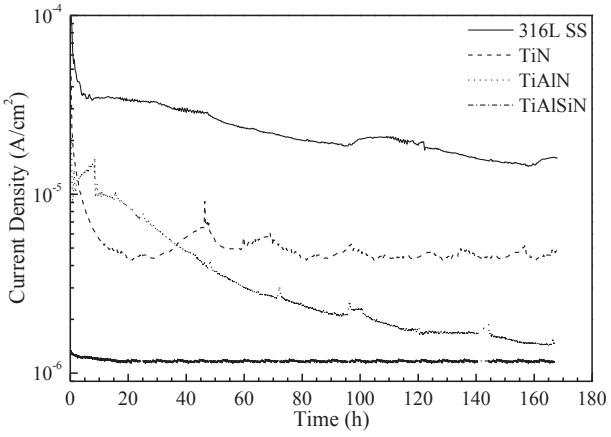

Fig. 7. Current density as a function of time in the simulated cathodic PEMFC environment under a constant applied potential of +600 mV_{SCE}.

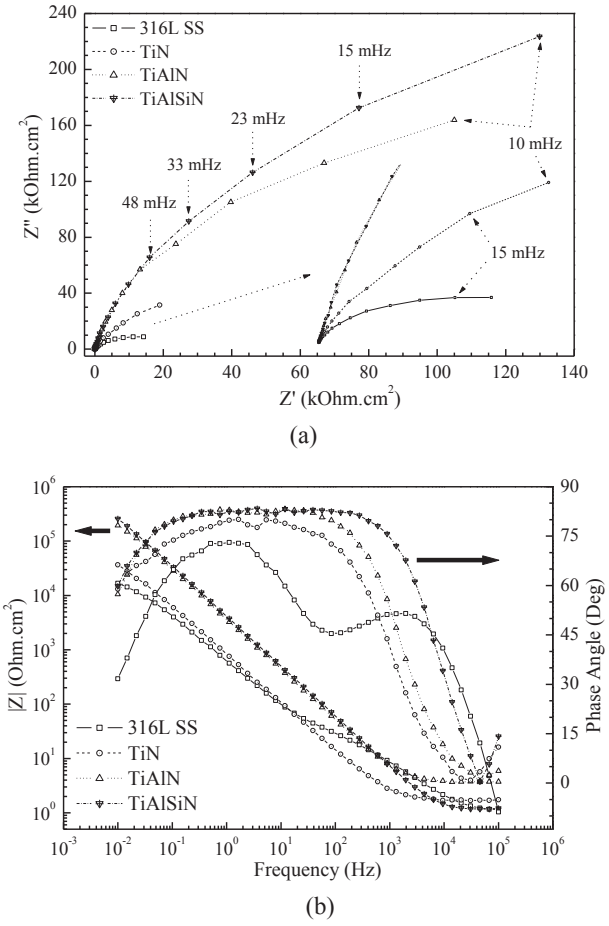

Fig. 8. Impedance spectra of the coating in (a) the Nyquist and (b) Bode plots.

corrosion. This means the coatings can effectively inhibit the inward penetration of F^-. The observed decrease in current density with Al and Si additions was due to the increased film stability, resulting in a high corrosion performance of the coatings. The potentiostatic test results confirmed the decrease in current density, which is in agreement with the polarization test results.

Fig. 8 shows the EIS results of the coating in the Nyquist and Bode plots. The impedance diagrams of the PANi-coated stainless steel showed much larger impedance than the bare 316L stainless steel as shown in Fig. 8(a). Fig. 8(b) shows Bode plots (impedance and phase angle vs. frequency) of the electrode for both the 316L SS substrate and the coatings after 24 h of +600 mV_{SCE} application.

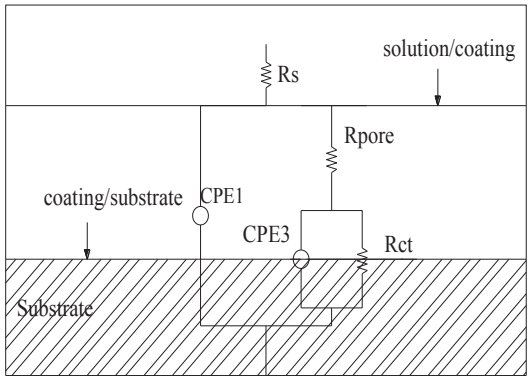

Fig. 9. Equivalent circuit for fitting the electrochemical impedance spectroscopy data.

Table 3
Fitted results of electrochemical impedance measurements (in case of 316L SS substrate, $R_{coating} = R_{film}$).

Specimen	R_s (Ω cm^2)	CPE1		$R_{coating}$ (Ω cm^2)	CPE2		R_{ct} (Ω cm^2)
		$C_{coating}$ (μF cm^{-2})	n (0 ~ 1)		C_{dl} (μF cm^{-2})	n (0 ~ 1)	
316L SS	1.2	104.0	0.8009	0.04E4	132.0	0.7558	2.31E4
TiN	1.8	0.9	0.9256	1.10E4	124.5	0.7964	1.13E5
TiAlN	1.7	0.5	0.9848	4.22E4	113.3	0.8296	4.67E5
TiAlSiN	1.8	0.2	0.9876	8.74E4	10.2	0.8913	7.30E5

The high frequency spectra shows the local surface defects, the medium frequency spectra are related to the processes within the coating, and the low frequency spectra indicate the processes at the metal/coating interface. The data typically showed a two-phase constant. Fig. 9 shows the corresponding equivalent circuit, where R_s represents the solution resistance between the reference and working electrodes, CPE1 denotes the constant phase element of the coating, R_{coat} is the coating resistance, R_{ct} is the charge transfer resistance, and CPE2 is the constant phase element of the double layer. R_s measured at the high frequency region can be subtracted from the sum of R_p ($R_p = R_{pore} + R_{ct}$) and R_s at the low frequency region to obtain the compensated R_{ct} value that is free of ohmic interference [50,51]. The coatings exhibited a high coating and charge transfer resistance, indicating a low corrosion rate, as shown in Table 3. The charge transfer resistance increased when Al and Si added to TiN coating. Overall, multicomponent hard coating TiAlSiN provides the best protection by improving the corrosion resistance of TiN coating and 316L SS substrate under simulated cathodic condition of PEMFC. It is related to the multicomponent hard coating controlled by interaction of the Al and Si with the TiN coating as a result of the corrosion barrier layer.

4. Conclusion

The TiAlSiN film deposited shows the strongest crystalline-refined TiN(200), highest hardness, and the improved surfaces roughness comparison with TiN and TiAlN. It could be attributed, on the basis of the Hall–Petch relationship, to the crystal size refinement due to the incorporation of Al and Si in TiN coating. The TiN, TiAlN and TiAlSiN coatings satisfied the quality requirement for BPs (<0.01 Ω cm^2) and should be more conducting in acidic environments, particularly in the cathode side of a PEMFC due to the decreased surface resistance after the potential loads. All of the coatings developed a passive film with a low passive current density. The protective efficiency was increased by the incorporation of Al and Si in TiN coating, indicating the improved corrosion resistance. The TiAlSiN-coated 316L SS exhibited a better corrosion resistance, coating performance, electrical resistance and conductivity on the cathode side of a PEMFC, in comparison with TiN, TiAlN-coated 316L SS and 316L SS substrate.

Acknowledgment

The authors are grateful for the support of Vietnam Oil and Gas Group, PetroVietnam University and the National Foundation for Sciences and Technology Development (NAFOSTED 2014).

References

[1] J. Jayaraj, Y.C. Kim, K.B. Kim, H.K. Seok, E. Fleury, Sci. Technol. Adv. Mater. 6 (2005) 282–289.
[2] E.A. Choa, U.S. Jeon, S.A. Hong, I.H. Oh, S.G. Kang, J. Power Sources 142 (2005) 177–183.
[3] H. Tsuchiya, O. Kobayashi, Int. J. Hydrogen Energy 29 (2004) 985–990.
[4] A. Hermann, T. Chaudhuri, P. Spagnol, Int. J. Hydrogen Energy 30 (2005) 1297–1302.
[5] R.C. Makkus, A.H.H. Janssen, F.A. de Bruijn, R.K.A.M. Mallant, Fuel Cell Bull. 3 (2000) 5–9.
[6] D.P. Davies, P.L. Adcock, M. Turpin, S.J. Rowen, J. Appl. Electrochem. 30 (2000) 101–105.
[7] A.K. Iversen, Corros. Sci. 48 (2006) 1036–1058.
[8] H. Wang, J.A. Turner, J. Power Sources 128 (2004) 193–200.
[9] H. Wang, G. Teeter, J. Turner, J. Electrochem. Soc. 152 (2005) B99–B104.
[10] N. Aukland, A. Boudina, D. Eddy, J. Mantese, M. Thompson, S. Wang, J. Mater. Res. 19 (2004) 1723–1729.
[11] R.F. Silva, D. Franchi, A. Leone, L. Pilloni, A. Masci, A. Pozio, Electrochim. Acta 51 (2006) 3592–3598.
[12] A. Pozio, F. Zaza, A. Masci, R.F. Silva, J. Power Sources 179 (2008) 631–639.
[13] R.C. Makkus, A.H.H. Janssen, F.A.D. Bruijn, R.K.A.M. Mallant, J. Power Sources 86 (2000) 274–282.
[14] D.P. Davies, P.L. Adcock, M. Turpin, S.J. Rowen, J. Power Sources 86 (2000) 237–242.
[15] N.D. Nam, J.G. Kim, W.S. Hwang, Thin Solid Films 517 (2009) 4772–4776.
[16] Y. Wang, D.O. Northwood, J. Power Sources 165 (2007) 293–298.
[17] Y. Wang, D.O. Northwood, Int. J. Hydrogen Energy 32 (2007) 895–902.
[18] W.S. Jeon, J.G. Kim, Y.J. Kim, J.G. Han, Thin Solid Films 516 (2007) 3669–3672.
[19] N.D. Nam, J.G. Kim, P.H. Tai, D.H. Yoon, J. Korean Phys. Soc. 54 (2009) 1104–1108.
[20] N.D. Nam, J.G. Kim, Jpn. J. Appl. Phys. 47 (2008) 6887–6890.
[21] Y. Fu, M. Hou, G. Lin, J. Hou, Z. Shao, B. Yi, J. Power Sources 176 (2008) 282–286.
[22] N.D. Nam, I.J. Park, J.G. Kim, Phys. Scr. T139 (2010) 014016-1–14021-5.
[23] R. Tian, J. Sun, J. Wang, Int. J. Hydrogen Energy 33 (2008) 7507–7512.
[24] N.D. Nam, J.H. Han, J.G. Kim, P.H. Tai, D.H. Yoon, Thin Solid Films 518 (2010) 6598–6603.
[25] H.S. Choi, D.H. Han, W.H. Hong, J.J. Lee, J. Power Sources 189 (2009) 966–971.
[26] N.D. Nam, K.H. Kim, J.G. Kim, Thin Solid Films 519 (2011) 6787–6791.
[27] Z. Li, K. Feng, Z. Wang, X. Cai, C. Yao, Y. Wua, Int. J. Hydrogen Energy (2014), http://dx.doi.org/10.1016/j.ijhydene.2014.03.136.
[28] N.D. Nam, M.J. Kim, D.S. Jo, J.G. Kim, D.H. Yoon, Thin Solid Films 545 (2013) 380–384.
[29] M.A. Lucio Garcia, M.A. Smit, J. Power Sources 158 (2006) 397–402.
[30] S. Joseph, J.C. McClure, R. Chianelli, P. Pich, P.J. Sebastian, Int. J. Hydrogen Energy 30 (2005) 1339–1344.
[31] Y. Wang, D.O. Northwood, J. Power Sources 163 (2006) 500–508.
[32] Y. Wang, D.O. Northwood, J. Power Sources 175 (2008) 40–48.
[33] N.D. Nam, J.G. Kim, Y.J. Lee, Y.K. Son, Corros. Sci. 51 (2009) 3007–3013.
[34] S. Carvalho, E. Ribeiro, L. Rebouta, C. Tavares, J.P. Mendonca, A.C. Monteiro, N.J.M. Carvalho, J.Th.M.D. Hosson, A. Cavaleiro, Surf. Coat. Technol. 177–178 (2004) 459–468.
[35] S. Zhang, D. Sun, X.L. Bui, in: S. Zhang, N. Ali (Eds.), Nanocomposite Thin Films and Coatings, Imperial College Press, London, 2007, ISBN 978-1-86094-784-1, pp. 1–110.
[36] D. Rafaja, A. Poklad, V. Klemem, G. Schreiber, D. Heger, M. Sima, Mater. Sci. Eng. A 462 (2007) 279–282.
[37] P. Holubar, M. Jilek, M. Sima, Surf. Coat. Technol. 133-134 (2000) 145–151.
[38] S. Vepřek, S. Reiprich, Li Shizhi, Appl. Phys. Lett. 66 (1995) 2640–2643.
[39] Y.Y. Chang, S.M. Yang, Thin Solid Films 518 (2010) 534–536.
[40] Yin-Yu Chang, Hsing-Ming Lai, Surf. Coat. Technol. (2014), http://dx.doi.org/10.1016/j.surfcoat.2014.02.015.
[41] D. Rafaja, M. Dopita, M. RŮžička, V. Klemm, D. Heger, G. Schreiber, M. Šíma, Surf. Coat. Technol. 201 (2006) 2835–2843.
[42] D. Rafaja, A. Poklad, V. Klemm, G. Schreiber, D. Heger, M. Ším, M. Dopita, Thin Solid Films 514 (2006) 240–249.
[43] Y.H. Yoo, D.P. Le, J.G. Kim, S.K. Kim, P.V. Vinh, Thin Solid Films 516 (2008) 3544–3548.
[44] V. Godinho, T.C. Rojas, S. Trasobares, F.J. Ferrer, M.P. Delplancke-Ogletree, A. Fernández, Microsc. Microanal. 18 (2012) 568–581.
[45] S.M. Yang, Y.Y. Chang, D.Y. Lin, D.Y. Wang, J. Nanosci. Nanotechnol. 9 (2009) 1108–1112.
[46] M. Diserens, J. Patscheider, F. Levy, Surf. Coat. Technol. 108–109 (1998) 241–246.
[47] A.H. Cottrell, An Introduction to Metallurgy, Edward Arnold, London, 1967, p. 394.
[48] G.S. Kim, B.S. Kim, S.Y. Lee, J.H. Hahn, Thin Solid Films 506–507 (2006) 128–132.
[49] N.D. Nam, J.H. Ahn, N.E. Lee, J.G. Kim, Mater. Res. Bull. 45 (2010) 269–274.
[50] J.R. MacDonald, Impedance Spectroscopy, Wiley, New York, 1987.
[51] D.C. Silverman, in: J.R. Scully, D.C. Silverman, M.W. Kendig (Eds.), Electrochemical Impedance: Analysis and Interpretation, ASTM STP 1188, American Society for Testing and Materials, Philadelphia, 1993.